AIP Applied Physics Letters

Diaphragm shape effect on the sensitivity of surface acoustic wave based pressure sensor for harsh environment

Tao Wang, Xiaojing Mu, Andrew Benson Randles, Yuandong Gu, and Chengkuo Lee

Citation: Applied Physics Letters **107**, 123501 (2015); doi: 10.1063/1.4931363
View online: http://dx.doi.org/10.1063/1.4931363
View Table of Contents: http://scitation.aip.org/content/aip/journal/apl/107/12?ver=pdfcov
Published by the AIP Publishing

Diaphragm shape effect on the sensitivity of surface acoustic wave based pressure sensor for harsh environment

Tao Wang,[1,2,3] Xiaojing Mu,[3,4,a)] Andrew Benson Randles,[3] Yuandong Gu,[3] and Chengkuo Lee[1,2,a)]

[1]*Department of Electrical and Computer Engineering, National University of Singapore, 4 Engineering Drive 3, Singapore 117583*
[2]*Center for Sensors and MEMS, National University of Singapore, 4 Engineering Drive 3, Singapore 117583*
[3]*Institute of Microelectronics (IME), Agency for Science, Technology and Research (A*STAR), 11 Science Park Road, Singapore 117685*
[4]*Key Laboratory of Optoelectronic Technology & Systems, Ministry of Education, Chongqing University, Chongqing 400044, People's Republic of China*

(Received 24 June 2015; accepted 7 September 2015; published online 21 September 2015)

Aluminum Nitride (AlN) based surface acoustic wave (SAW) pressure sensors for harsh environment applications are of great interest in recent years. Such sensor employs a thick diaphragm ($\sim$50 μm) to endure the high pressure, but this seriously limits the sensitivity of these devices. Understanding of the working mechanism and the effect of geometrical parameters will yield the design principles to achieve improved sensitivity. In this letter, the effect of diaphragm on the performance of SAW pressure sensors is studied. AlN based SAW resonators on (100) wafer with different diaphragm shapes are fabricated, packaged, and characterized. Pressure coefficient of frequency (PCF) of pressure sensors with circular diaphragm, rectangular diaphragm (small aspect ratio) and rectangular diaphragm (large aspect ratio) is found to be 0.071 ppm/psi, 0.038 ppm/psi, and $-$0.171 ppm/psi, respectively. The longitudinal and lateral strains along the SAW propagation direction ($\langle 100 \rangle$ direction) have the opposite effects on the frequency change, i.e., longitudinal strain increases the resonant frequency while lateral strain decreases the resonant frequency. Hence, the measured PCF is a combined effect of the two strains, whereby increase in lateral strain results in lower PCF. The ratio of longitudinal/lateral strain is determined by the diaphragm shape. The rectangular diaphragm (large aspect ratio) with only lateral strain thus shows negative PCF. Additionally, by changing the wafer plane, SAW propagation direction and ratio of longitudinal/lateral strains may help to enhance the primary strain effect and minimize the reverse strain effect. This approach could further improve the sensitivity of pressure sensor without sacrificing its high pressure sensing range for harsh environment applications. © *2015 AIP Publishing LLC*.
[http://dx.doi.org/10.1063/1.4931363]

Pressure sensor is the most widely used microelectromechanical system (MEMS) device in the market.[1] Several harsh environment application areas, like automotive, aeronautic, and oil-drilling industry, desire to have miniaturized pressure sensors with low power consumption, improved sensitivity, and stability at high temperature and high pressure environment.[2–10] However, MEMS based sensing technology for such applications is not readily available; hence, pressure sensor for harsh environment is gaining increased research interest recently. Traditional silicon based piezoresistive pressure sensor can barely be employed in high temperature environment due to severe degradation in its accuracy and sensitivity.[11] Though SiC based pressure sensor for high temperature (>300 °C) application has been demonstrated, the accuracy is not satisfactory at high temperature and the cost is considerably high.[12,13] Another approach for high temperature operation falls on quartz based resonators, which have been popularly used as high pressure sensors in harsh environment for a long time.[14,15] However, quartz based resonator still suffers from considerable performance degradation due to the piezoelectric coefficient loss for temperature higher than 250 °C.[16] Alternatively, aluminum nitride (AlN) based acoustic wave pressure sensor has been reported to provide high stable performance at high temperature,[17] and the piezoelectric coefficient of AlN remains relatively unaffected with increasing temperature. In addition, AlN is a complementary metal-oxide-semiconductor (CMOS) compatible material and so enables high volume batch fabrication with potentially low cost as it can be monolithically integrated with sensors and integrated circuits (IC).[18,26,27] However, the temperature induced frequency drift is still significant in these devices, which may largely affect the sensor accuracy. In order to eliminate the adverse effect of temperature on the sensor performance, a dual mode acoustic wave pressure sensor has also been reported.[19] By temperature cancellation from the two modes, very accurate and solo pressure readout is achieved. Hence, AlN based acoustic pressure sensor is proven to be stable, accurate, and a low-cost solution, especially for high temperature applications.

Besides the high temperature, high pressure is another concern for harsh environment applications. To fulfill the

a)Authors to whom correspondence should be addressed. Electronic addresses: mxjacj@outlook.com and elelc@nus.edu.sg

high pressure requirement, previously reported AlN based acoustic pressure sensors employ relatively thick diaphragm. For the pressure sensing range of 300 psi or even higher, thick diaphragms of 30 μm or 50 μm are used, and this adversely affects the sensitivity of these devices.[19] Therefore, to enhance the sensitivity of such pressure sensors is in great demand. Unfortunately, the study of the sensitivity mechanism of AlN based acoustic wave pressure sensor for harsh environment applications has not been reported till date.

In this letter, AlN based surface acoustic wave (SAW) pressure sensors with different diaphragm shapes are developed, packaged, and characterized. The sensors with circular and rectangular (small aspect ratio) diaphragms are found to provide positive pressure coefficient of frequency (PCF), while the sensor with rectangular diaphragm (large aspect ratio) shows negative PCF. Acoustoelastic effect plays a critical role in this pressure sensitivity difference. Longitudinal and lateral strains along SAW propagating direction have opposite contributions to the frequency change, and hence, the sensor with rectangular diaphragm (large aspect ratio), which is laterally strained, shows the negative PCF. This work also indicates approaches to further improve the sensitivity of AlN based SAW pressure sensors for harsh environment applications.

3-D illustrations of the AlN based SAW pressure sensor is shown in Figure 1(a). AlN thin film is adopted as the piezoelectric layer and the bottom Molybdenum (Mo) electrode helps to increase the electromechanical coupling efficiency. A set of interdigital transducer (IDT) electrodes (50 pairs) made of Mo with 10.4 μm periodicity is used for inducing SAWs. Propagating SAWs are reflected by the two Bragg reflectors placed on either side of the IDT electrodes and this gives rise to resonant modes. The 50 μm thick supporting silicon layer aims to fulfill the high pressure requirement. To study the influence of diaphragm shape on sensitivity, three different pressure sensors are designed: circular diaphragm with diameter of 800 μm (PS_A), rectangular diaphragm with size of 1000 μm $\times$ 800 μm (PS_B), and rectangular diaphragm with size of 2700 μm $\times$ 800 μm (PS_C). The three sensors share the same resonator design but different diaphragm shapes. Corners of rectangular diaphragm are rounded to avoid the high localized stress, making the sensors more reliable.

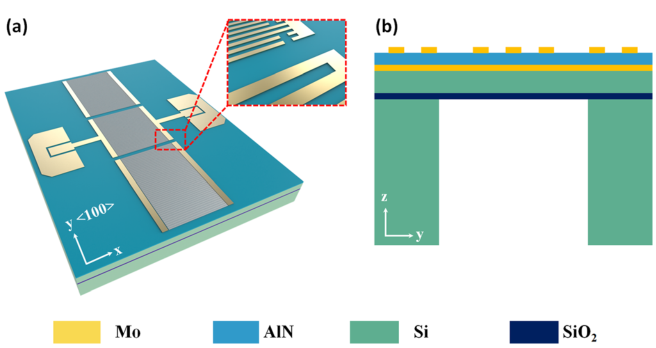

FIG. 1. (a) The 3-D schematic illustration of the AlN based SAW pressure sensor; (b) cross-sectional view of the illustration. All the devices are fabricated on (100) wafer and the SAW propagating direction is along ⟨100⟩.

The fabrication process starts from an 8 in. SOI (100) wafer with 50 μm device layer and 5 μm buried oxide (BOX) layer. Prior to the deposition of Mo/AlN/Mo stack, a 20 nm AlN seeding layer is grown by atomic layer deposition (ALD). Next the physical vapour deposition (PVD) is used to deposit the 0.2 μm Mo/1.2 μm AlN/0.2 μm Mo stack on the AlN seeding layer. The top Mo layer is patterned using plasma enhanced chemical vapour deposition (PECVD) silicon dioxide (SiO_2) as the hard mask. A layer of 0.4 μm PECVD SiO_2 layer is then deposited for isolation. This SiO_2 is etched and followed by AlN etching to open the Bottom Mo-to-Top Metal via. Top Mo-to-Top Metal via is opened by SiO_2 patterning as well. Subsequently, a 0.7 μm Al is deposited and patterned to form the electrical connections and bonding pads. Finally, the diaphragm is released by backside deep reactive ions etching (DRIE). The as-fabricated pressure sensors are shown in Figures 2(a) and 2(b). Figure 2(c) shows the backside cavities and the differently shaped diaphragms.

The fabricated pressure sensors are then packaged and assembled with printed circuit board (PCB) for testing as shown in Figure 2(d). Since the pre-defined wavelength by IDT is 10.4 μm, which is 1/5 less than the thickness of diaphragm ($\sim$56 μm), SAW is expected to be induced. Agilent E5071B network analyzer is employed to measure the S parameters. Short-Open-Load-Through (SOLT) method is performed before testing to calibrate out the parasitic parameters introduced by PCB and bonding wires. The S21 parameter of the pressure sensor is extracted first and shown in Figure 3(a). Because the pressure sensors share the same resonator design, their behaviors without applying pressure are the same. This pressure sensor resonates at 432.29 MHz. Considering the pre-defined wavelength of 10.4 μm, the phase velocity of the acoustic wave is derived as 4495.8 m/s. Such low velocity implies that the induced acoustic wave is a SAW, i.e., Rayleigh wave, which is expected.[19] A 2-D finite element analysis (FEA) model is also built by COMSOL Multiphysics software, using the Piezoelectric Devices

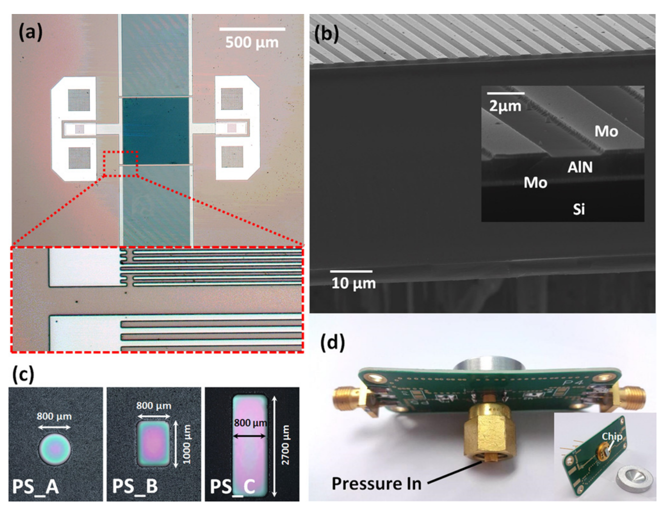

FIG. 2. (a) Optical microscope (OM) image of fabricated pressure sensor; secondary electron microscope (SEM) images, showing the 50 μm thick silicon layer; (c) backside view of the three pressure sensors showing the different diaphragm shapes; and (d) packaged and assembled pressure sensor with PCB for testing. The pressure is applied using hydraulic controller through the tube and the SMA connectors are for signal readout.

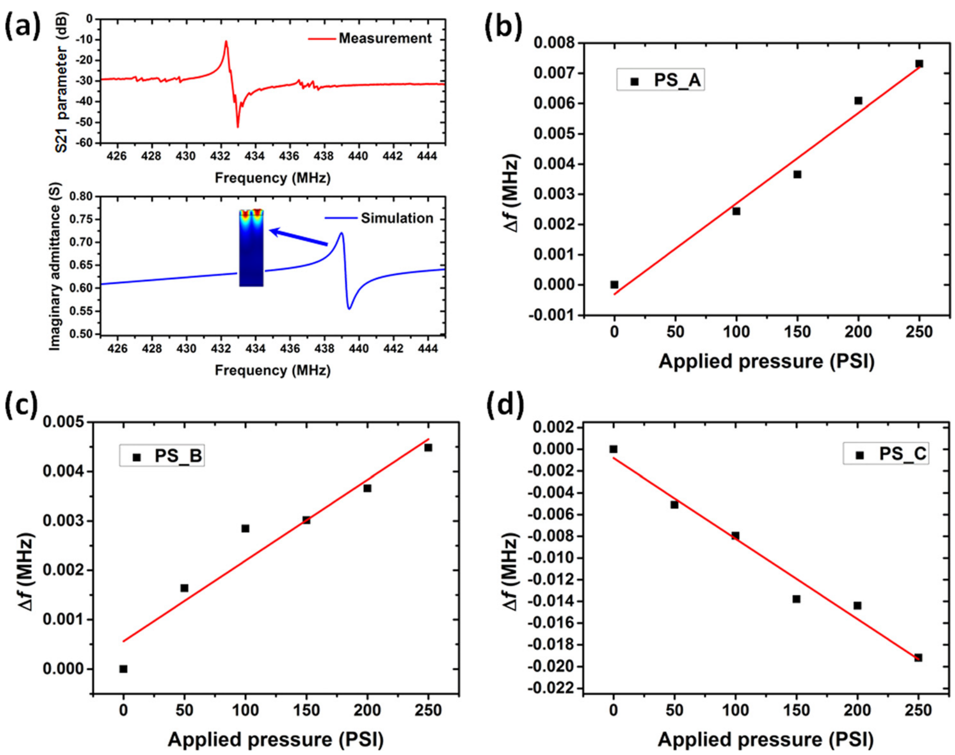

FIG. 3. (a) Measured and simulated frequency responses of the pressure sensor. The mode shape indicates the induced acoustic wave is a SAW; and (b)–(d) the frequency change with respect to applied pressure for PS_A, PS_B, and PS_C, respectively.

model with Frequency Domain study. The simulated imaginary admittance of the resonator is shown in Figure 3(a) as well, where the resonant frequency is 438.97 MHz and slightly higher than the measured result. The mode shape clearly shows that the induced acoustic wave is a SAW, and most of the displacement is confined within the depth of one wavelength near the surface.

Pressure is then applied to the sensors from backside using hydraulic pressure controller from 0 to 250 psi. Even though the sensors function well at pressure over 700 psi, a relatively lower pressure is applied to minimize the sensitivity change due to non-linear effects. Frequency changes with respect to the applied pressure are recorded and plotted in Figures 3(b)–3(d). The PCFs are derived as 0.071 ppm/psi (30.02 Hz/psi), 0.038 ppm/psi (16.36 Hz/psi), and −0.171 ppm/psi (−74.12 Hz/psi) for PS_A, PS_B, and PS_C, respectively. The sensitivity behaviors of the three sensors seem quite different. PS_A and PS_B have positive PCFs while PS_C has negative PCF, and PS_A is more sensitive than PS_B. To further investigate the mechanism behind such different sensitivity behaviors, another FEA model (Structural Mechanical Model) is built, and all the diaphragms are applied with 250 psi pressure. The Von Mises stress distributions are shown in Figure 4(a), and the associated strain directions are shown in Figure 4(b). Since only the portion of diaphragm near the top surface displaces when SAW is propagating, the stresses and strains on the top surface are considered because they primarily affect the SAW phase velocity. Red and blue arrows represent for the tensile and compressive strains, respectively, and the dash lines indicate where the IDTs are located. It is clearly shown that the IDTs in all three devices are bearing the same type of strain, i.e., the tensile strain. Thus, the negative PCF for PS_C should not be caused due to the type of strain. Furthermore, PS_A shows less strain than PS_B, and hence, the higher PCF of PS_A should not be caused due to larger strain. Thus, the measured PCF variation for different diaphragm should be attributed to other non-obvious effects.

The frequency of a SAW resonator can be described as

$$f_{SAW} = \frac{v_{ph}}{\lambda}, \qquad (1)$$

where v_{ph} is the phase velocity and λ is the wavelength of the SAW. For the wavelength, which is determined by IDT periodicity, it may slightly change because of the strain. As all three pressure sensors are bearing tensile strain, the elongation in IDT will only result in a lower resonant frequency. However, both of PS_A and PS_B show a positive PCF, implying that the wavelength change may not be the major effect, but the phase velocity effect dominates the frequency

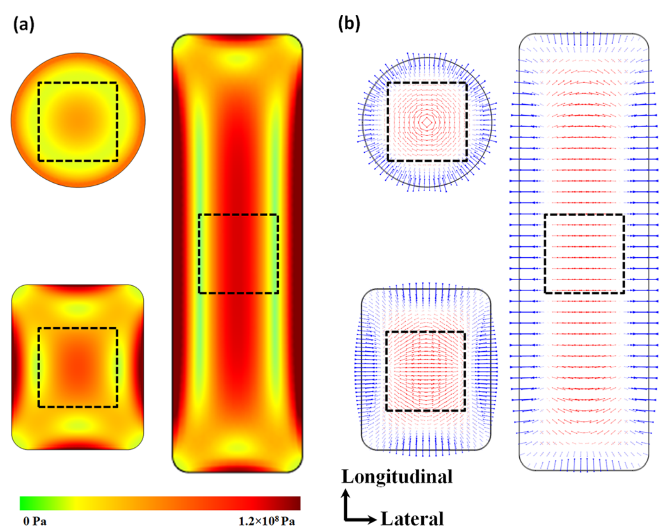

FIG. 4. (a) Simulated Von Mises stress distributions of the three pressure sensors; and (b) the associated strain directions of the three pressure sensors. The dashed lines indicate where the IDTs are located.

change. In order to take the initial strain into account and obtain the phase velocity of SAW, a form of equations of motion is used as[20]

$$\frac{\partial}{\partial x_i}[\sigma_{ik}u_{j,k} + T_{ij}] = \rho\frac{\partial^2 u_j}{\partial t^2}. \tag{2}$$

Considering a piezoelectric medium, this equation becomes[21]

$$\sigma_{ik}u_{j,ki} + c_{ijkl}u_{k,li} + e_{kij}\phi_{,ki} = \rho\frac{\partial^2 u_j}{\partial t^2}, \tag{3}$$

$$e_{ikl}u_{k,li} + \epsilon_{ik}\varphi_{,ki} = 0, \tag{4}$$

where σ is the initial stress, u the mechanical displacement, ρ the density, c the elastic moduli, e the piezoelectric moduli, ϵ the permittivity tensors, and φ the electric potential. The subscripts $i, j, k,$ and l take on the values 1, 2, and 3. Since acoustoelastic effect plays an important role in the phase velocity change, strain induced elastic moduli change must be considered. Thus the higher-order elasticity is introduced, and the stress-strain relation becomes non-Hookean as[22]

$$\sigma = c\varepsilon + \frac{1}{2}c'\varepsilon^2, \tag{5}$$

where σ is the stress, ε is the strain, c is the linear elastic moduli and c' is the third-order elastic moduli. The effective elastic moduli thus are strain-dependent and vary with increasing strain, changing the phase velocity. It is worth noting that the third-order elastic moduli of AlN can be ignored, because the bonds between crystallites in a thin polycrystalline film are very weak.[23] The third-order elastic moduli of Si, however, are very important and must be taken into consideration. Although the density of medium changes with strain as well (due to volume change), such effect only has minimum effect on the phase velocity based on previous study.[21] Hence, it is reasonable to neglect the density effect for our work.

Koleshko *et al*. have done a comprehensive study of strain effect of AlN based SAW device on silicon substrate.[24] Abovementioned set of equations are solved with boundary conditions using numerical method. Because silicon is a highly anisotropic material and its third-order elastic moduli are anisotropic as well,[25] the strain effect on phase velocity depends on the crystallographic plane of silicon wafer, direction of SAW propagation and direction of applied strain. The phase velocity after strain v_{ph} is defined as

$$v_{ph} = v_0(1 + \gamma\varepsilon), \tag{6}$$

where v_0 is the phase velocity with zero strain, and a coefficient γ is introduced to describe the velocity sensitivity to strain. Since all the pressure sensors in this work are fabricated on a (100) Si wafer, the computation results for (100) Si plane are summarized in Table I. The longitudinal strain means a homogenous uniaxial tensile strain applied along with the direction of SAW propagation, while the lateral means a tensile strain perpendicular to the direction of SAW propagation. As is shown in Figure 1, the SAW propagates along $\langle 100 \rangle$ direction for all the pressure sensors. For such case, the longitudinal and lateral strains have opposite effects on the SAW phase velocity, i.e., longitudinal strain increases the velocity ($\gamma = 0.8$) while lateral strain decreases the velocity ($\gamma = -0.3$), as shown in Table I. This could be the reason for different sensitivity behaviors of these sensors.

TABLE I. Phase velocity sensitivity to strain γ for (100) Si plane.[24]

SAW propagation direction	Longitudinal strain	Lateral strain
$\langle 100 \rangle$	0.8	−0.3
$\langle 110 \rangle$	1.9	0.3

The strain directions of the three pressure sensors are shown in Figure 4(b). For the axially symmetric circular diaphragm (PS_A), it is equally strained in longitudinal and lateral directions. Due to the larger γ for longitudinal strain, the combined strain effect for PS_A is to increase the phase velocity, showing a positive PCF. Lateral strain effect cancels part of longitudinal strain effect, and results in lowering of the positive PCF compared to the one that only has longitudinal strain effect. The square diaphragm has the similar situation as the circular one, which also bears longitudinal and lateral strains of equal value. However, if the diaphragm is changed to rectangular shape, the strain starts becoming more lateral (PS_B). More lateral strain means the more significance of the cancellation effect. Though the combined strain effect still contributes to the increase of the velocity and frequency, PS_B shows a lower PCF than that of PS_A. As the aspect ratio of rectangular diaphragm increases, more region of diaphragm experiences the lateral strain (PS_C). It is clearly shown that the IDT of PS_C is entirely laterally strained, and thus, only lateral strain effect attributes to its velocity change. Without the longitudinal strain effect, PS_C therefore shows a negative PCF. It is worth noting that the absolute PCF of PS_A is lower than that of PS_C. This could probably be because of the following reasons: (1) PS_C has larger diaphragm and larger strain for same applied pressure; (2) longitudinal strain induced elongation of IDT periodicity decreases the frequency of PS_A, which partially cancels the strain effect on velocity (increasing frequency), while on the other hand, the lateral strain does not affect the IDT periodicity of PS_C and; (3) almost all strain for PS_C contributes to frequency decrease, while only half the induced strain in PS_A is longitudinal and contributes to the increase of the frequency.

As discussed above, the frequency change of pressure sensor is attributed to different effects. These effects may work against each other and result in a relatively low sensitivity. Enhancing the primary effect and minimizing the reverse effect may result in further increase in the sensitivity without sacrificing the diaphragm thickness, i.e., the high pressure sensing range. For axially symmetric diaphragm design (PS_A), in-plane tilting the position of the IDT and reflectors by 45° and generating SAW propagating along $\langle 110 \rangle$ direction can help to increase the PCF. In this case, the velocity sensitivities to longitudinal strain and lateral strain become 1.9 and 0.3, respectively. The lateral strain does not cancel the effect of longitudinal strain but slightly enhances it, giving rise to a larger frequency change. Another possible approach is rotating the diaphragm of PS_C by 90°.

TABLE II. Phase velocity sensitivity to strain γ for (110) Si plane.[24]

SAW propagation direction	Longitudinal strain	Lateral strain
⟨110⟩	1.8	−1.1
⟨100⟩	0.9	−0.05

The pressure induced strain becomes entirely longitudinal, resulting in a large positive PCF without cancellation from lateral strain effect. Finally, Table II summarizes the γ for (110) silicon plane. As the lateral strain does not change the IDT periodicity and affect the frequency for PS_C, if the silicon wafer is changed to (110), the maximum negative PCF may be achieved.

In conclusion, the influence of diaphragm shape on sensitivity of AlN based SAW pressure sensor is experimentally studied. Three pressure sensors with same SAW resonator design but different diaphragm shapes are fabricated, packaged, and characterized. The sensors with circular diaphragm, rectangular diaphragm with small aspect ratio, and rectangular diaphragm with large aspect ratio have PCFs of 0.071 ppm/psi, 0.038 ppm/psi, and −0.171 ppm/psi, respectively. The shape of the diaphragm influences the longitudinal/lateral strain ratio. Longitudinal and lateral strains have opposite effects on phase velocity and frequency change for (100) silicon plane along ⟨100⟩ propagation direction, and so results in different sensitivity behaviors. By changing the silicon wafer plane, SAW propagation direction, and longitudinal/lateral strain ratio, the reverse strain effect can be engineered. Hence, the sensitivity of the pressure sensor may be increased, without sacrificing its high pressure sensing range for harsh environment applications.

This work was supported by SERC of the Agency for Science, Technology and Research, Singapore under Grant No. 1220103064, and partially supported by MOE2012-T2-245 2-154 (Monolithic Integrated Si/AIN Nanophotonics Platform for Optical NEMS and OEICs) from the Ministry of Education- Singapore (MOE).

[1]S. Zhang, T. Wang, L. Lou, W. M. Tsang, R. Sawada, D.-L. Kwong, and C. Lee, J. Microelectromech. Syst. **23**(6), 1396 (2014).
[2]Y. Hezarjaribi, M. N. Hamidon, S. H. Keshmiri, and A. R. Bahadorimehr, paper presented at the IEEE International Conference on Semiconductor Electronics (2008).
[3]C. Kolle, W. Scherr, D. Hammerschmidt, G. Pichler, M. Motz, B. Schaffer, B. Forster, and U. Ausserlechner, in Proceedings of IEEE Sensors (2004).
[4]Y. Zhang, R. Howver, B. Gogoi, and N. Yazdi, paper presented at the 16th International Solid-State Sensors, Actuators and Microsystems Conference (2011).
[5]A. M. Anis, M. M. Abutaleb, H. F. Ragai, and M. I. Eladawy, paper presented at the Third International Conference on Computational Intelligence, Modelling and Simulation (CIMSiM) (2011).
[6]S. Dakshinamurthy, N. R Quick, and A. Kar, J. Appl. Phys. **99**(9), 094902 (2006).
[7]J. Xu, G. Pickrell, X. Wang, W. Peng, K. Cooper, and A. Wang, IEEE Photonics Technol. Lett. **17**(4), 870 (2005).
[8]L. S. Pakula, H. Yang, H. T. M. Pham, P. J. French, and P. M. Sarro, J. Micromech. Microeng. **14**(11), 1478 (2004).
[9]H. San, H. Zhang, Q. Zhang, Y. Yu, and X. Chen, J. Micromech. Microeng. **23**(7), 075020 (2013).
[10]X. Zhao, J. M. Tsai, H. Cai, X. M. Ji, J. Zhou, M. H. Bao, Y. P. Huang, D. L. Kwong, and Ai. Q. Liu, Opt. Express **20**(8), 8535 (2012).
[11]A. A. Ned, R. S. Okojie, and A. D. Kurtz, in *Fourth International High Temperature Electronics Conference* (HITEC) (1998), p. 257.
[12]R. S. Okojie, C. W. Chang, and L. J. Evans, J. Microelectromech. Syst. **20**(5), 1174 (2011).
[13]R. S. Okojie, A. A. Ned, and A. D. Kurtz, Sens. Actuators, A **66**(1), 200 (1998).
[14]R. J. Besson, J. J. Boy, B. Glotin, Y. Jinzaki, B. Sinha, and M. Valdois, IEEE Trans. Ultrason. Ferroelectr. Freq. Control **40**(5), 584 (1993).
[15]L. D. Clayton and E. P. EerNisse, IEEE Trans. Ultrason. Ferroelectr. Freq. Control **45**(5), 1196 (1998).
[16]E. P. EerNisse and R. B. Wiggins, IEEE Sens. J. **1**(1), 79 (2001).
[17]P. Kropelnicki, K. M. Muckensturm, X. J. Mu, A. B. Randles, H. Cai, W. C. Ang, J. M. Tsai, and H. Vogt, J. Micromech. Microeng. **23**(8), 085018 (2013).
[18]T. Wang, X. Mu, P. Kropelnicki, A. B. Randles, and C. Lee, J. Micromech. Microeng. **24**(7), 075002 (2014).
[19]X. Mu, P. Kropelnicki, Y. Wang, A. B. Randles, K. T. C. Chai, H. Cai, and Y. D. Gu, Appl. Phys. Lett. **105**(11), 113507 (2014).
[20]V. V. Bolotin, G. Herrmann, and T. K. Lusher, *Nonconservative Problems of the Theory of Elastic Stability* (Pergamon Press, Oxford, 1963).
[21]A. L. Nalamwar and M. Epstein, J. Appl. Phys. **47**(1), 43 (1976).
[22]M. Hirao and H. Ogi, *EMATs for Science and Industry: Noncontacting Ultrasonic Measurements* (Springer Science & Business Media, 2003).
[23]A. L. Nalamwar and M. Epstein, IEEE Trans. Sonics Ultrason. **23**, 144 (1976).
[24]V. M. Koleshko, Yu. V. Meshkov, and V. V. Barkalin, Thin Solid Films **190**(2), 359 (1990).
[25]P. N. Keating, Phys. Rev. **149**(2), 674 (1966).
[26]T. Wang and C. Lee, J. Microelectromechanical Systems **PP**(99), 1 (2015).
[27]T. Wang, R. Sawada, and C. Lee, IEEE Electron Device Letters **36**(9), 957–959 (2015).